Effects of Processing Parameters and Molecular Weight Distribution on the Tensile Properties of Polypropylene Fibers

ERIK ANDREASSEN,[1,*] OLE JAN MYHRE,[2] EINAR L. HINRICHSEN,[1] and KRISTIN GRØSTAD[2]

[1]Sintef, P.O. Box 124 Blindern, N-0314 Oslo, Norway; [2]Statoil, N-3960 Stathelle, Norway

SYNOPSIS

The tensile properties of polypropylene fibers, produced in a short-spin line, are correlated with the parameters of the three processing stages (spinning, drawing, and annealing), and with the molecular weight distribution. In general, tensile stiffness and strength increase with increasing molecular orientation, while the elongation at break decreases. The degree of orientation is determined by the deformation ratios and temperatures of the first two stages. Tensile modulus and strength also increase with increasing annealing stage shrinkage ratio. All the tensile properties, including the elongation at break, increase with increasing average molecular weight. The mechanisms of crystallization and deformation are related to the molecular weight distribution in different ways. Hence, the tensile modulus is highest for broad distributions when the draw ratio is low, and for narrow distributions when the draw ratio is high. The tensile strength increases and the elongation at break decreases as the width of the molecular weight distribution decreases, for all combinations of processing parameters. The distribution of tensile strength, for fibers with high draw ratios, broadens as the molecular weight distribution narrows. The total draw ratio of fibers, as experienced during processing and testing, and the true stress at break, are discussed in terms of deformation rates and relaxation times. © 1994 John Wiley & Sons, Inc.

1. INTRODUCTION

The tensile properties of polypropylene (PP) fibers are highly correlated with the molecular orientation in crystalline and noncrystalline regions. It is well known that tensile modulus, yield stress, and tensile strength increase with increasing orientation, while the elongation at break decreases. The orientation is a result of the total thermomechanical history of the fiber, which can be described as a combination of deformation ratios, rates, and temperatures. Available processes offer a wide range of fiber diameters and tensile properties. This article is based on results from the short-spin process (also known as compact spinning), but most of the findings apply to other processes as well. The short-spin line consists of three integrated stages: spinning, drawing, and annealing. Typical fibers produced by this process have tensile modulus in the range 0.5–3.0 GPa, tensile strength in the range 50–600 MPa, and elongation at break in the range 50–600%.

Most of the literature dealing with the tensile properties of PP fibers focuses on the spinning stage of the long-spin process (also known as conventional spinning).[1–5] The literature on the effects of drawing and annealing on the tensile properties is sparse, but there is a number of articles that discuss the structure development in these stages.[6–11] Some relevant articles on tensile properties vs. drawing conditions can be found among the vast literature on polyethylene (PE) fibers.[12–15]

The major differences between short-spin and long-spin processes are summarized in the Appendix, which also contains definitions of processing parameters and a list of symbols.

2. EXPERIMENTAL

Fibers with circular cross-section were produced in a Barmag FE1 full-scale short-spin line, and a spin-

* To whom correspondence should be addressed.

Journal of Applied Polymer Science, Vol. 52, 1505–1517 (1994)
 CCC 0021-8995/94/101505-13

neret with 9000 holes with radius 0.2 mm was used. A reduced factorial design was employed for the variation of molecular weight characteristics and typical industrial processing parameters, cf. Table I. The polymers in this study are homopolymers with isotactisity in the range 96–98%. Two different commercial additive systems have been used. One of them is known to have a nucleating effect under quiescent conditions. Lu and Spruiell[16] recently reported effects of nucleating agents on the properties of PP fibers spun at low spinline stresses. However, no significant differences were observed between the additive systems used in our study.

For a given polymer and processing condition, the velocity of the cooling air was adjusted somewhat in order to avoid filament breakage in the spinning stage. With this adjustment, the distance from the die to the solidification point varies less from one set of spinning parameters to another. The effects of extrusion temperature and draw-down ratio (the ratio of spinning velocity to extrusion velocity) are still present, and, for a given draw-down ratio, the elongation rate varies less with other spinning parameters.

Linear density and tensile properties of the fibers were measured with a Lenzing Vibroskop/Vibrodyn instrument at ambient temperature. Fibers with initial gauge length 1 cm were stretched at a crosshead speed of 5 cm/min. If not otherwise stated, the reported stress is nominal, i.e., load divided by initial cross-sectional area. Nominal stress of fibers is usually called tenacity when it is measured as load divided by linear density (e.g., with units N/tex, 1 tex = 1 g/km).[17] The tensile modulus was calculated by fitting a straight line through origo and the average stress at 1, 2, and 3% elongation. The structure and molecular orientation of the fibers were also analyzed by birefringence, wide angle x-ray scattering (WAXS), infrared (IR) spectroscopy, differential scanning calorimetry (DSC), and density measurements.

Table I Parameters for Molecular Weight Distribution (as Determined by SEC) and Processing Conditions, with Associated Ranges, as Examined in this Study

M_w[a]	160,000–230,000
M_w/M_n	3.4–5.8
Extrusion velocity	0.15 m/min–0.9 m/min
Extrusion temperature	220°C–280°C
Spinning velocity	10 m/min–50 m/min
Draw ratio	1.2–3.5
Drawing temperature	20°C–180°C
Annealing ratio	2%–7%
Annealing temperature	150°C–180°C
Line velocity	40 m/min–70 m/min
Final fiber dimension	4 dtex–11 dtex

[a] The melt flow indices were in the range 8–25.

The reproducibility of the process and the tensile testing was assessed by producing three sets of some of the fibers. Between these productions, the fiber line was started, adjusted, and stopped several times. The set-to-set variations in measured tensile strength and elongation at break were less than 4%. Some of the fibers with the highest expected degradation during processing were analyzed by size exclusion chromatography (SEC). The change in M_w was always less than 5%.

Stress–strain curves in the literature are either selected as representative for the parallels tested or obtained from all the parallels by an averaging procedure. Mechanical data and stress–strain curves presented in this article are the average of about 20 parallels. "Average" stress–strain curves can be produced in different ways. The problem is, of course, that the parallels have different elongation and tenacity at break. The simplest procedure is just to add the stress–strain parallels (for each elongation) and divide the sum by the number of parallels that are contributing, i.e., with elongation at break above the elongation in question. However, at high elongations, only a few parallels will contribute, and the average curve will be discontinous at the elongation at break of each parallel. Hence, the tenacity at break of this average curve will be equal to the tenacity at break of the parallel with the highest elongation at break (when elongation is the independent variable).

The average stress–strain curves shown in this article are produced by the following procedure:

1. Average elongation at break (ϵ_b) and tenacity at break (σ_b) are calculated.
2. The stress–strain curve of each parallel is scaled by multiplicative factors, in order to end at the point (ϵ_b, σ_b).
3. The average curve is calculated from the scaled curves.

The ideal averaging procedure would take the average of actual curves at low elongations, and of scaled curves at high elongations. However, for most fibers, the average stress–strain curve of scaled parallels represents the average fiber response well. Applying this averaging procedure is simpler than selecting a representative parallel, and the latter will

not have the exact average elongation and tenacity at break. A simple test of this scaling method is to "reconstruct" the parallels, by scaling the average curve to ϵ_b and σ_b of the parallels. In most cases, the reconstructed curves closely resemble the originals. The elongation at yield differ more among the reconstructed curves than among the original parallels, but this effect is only significant when ϵ_b of the reconstructed curve is low. Hence, our conclusion is that this scaling procedure is a simple way of producing stress–strain curves that represent the average stress–strain relationship of fibers well. More details of the scaling procedure, and some further applications, will be given in a forthcoming article, dealing with the tensile response of fiber assemblies.

3. RESULTS AND DISCUSSION

3.1. Effects of Processing Parameters

3.1.1. Spinning Stage Parameters

As mentioned earlier, the short-spin line used in this study consists of three integrated stages: spinning, drawing, and annealing. In the spinning stage, the extruded melt is subjected to elongational deformation. The filaments are cooled by turbulent air, and solidify a few centimeters below the die. WAXS data indicate that there are two spinning regimes:

Regime I. Above a critical spinline stress, monoclinic α phase with bimodal orientation is obtained. The molecular orientation in crystalline and noncrystalline regions, and the degree of crystallinity increase with increasing spinline stress, i.e., the crystallization is stress-induced:[18] the reduction of the entropy in the strained melt leads to an increased crystallization temperature. The bimodal orientation in PP fibers is well known. Katayama et al.[19] showed that the secondary population (with chains oriented perpendicular to the fiber axis) nucleates after the primary population (with chains oriented parallel to the fiber axis). One possible explanation for the formation of two distinct populations is that after some time row nuclei carry so much of the tensile load that the melt between them can relax.[18] The molecular origin of the autoepitaxy has been discussed by Lotz and Wittmann.[20] The fraction of chains in the secondary population increases with increasing spinline stress. However, the average angle between the fiber axis and a polymer chain (e.g., measured by IR dichroism) decreases with increasing spinline stress, because the increase in the orientation of the primary population dominates the effect of the fractional decrease in this population.

Regime II. Below a critical spinline stress, a uniaxially oriented mesomorphic phase is obtained. The degree of orientation is less than in regime I. The mesomorphic phase can be considered as intermediate between the amorphous state and the α phase, and it is found in quenched samples.[21] In our case, the spinline stress is probably too low for stress-induced crystallization to dominate. On the other hand, the cooling rate is too high for the molecules to organize into well-ordered crystallites from the relatively unoriented melt.

For a certain polymer grade, the spinline stress increases with decreasing extrusion temperature and increasing draw-down ratio. Because the draw ratio is the dominant processing variable (discussed below), the effects of the spinning stage are most significant when the draw ratio is low. In this case, the tensile properties of fibers produced in regime I are superior to those in regime II (when the molecular weight distribution is the same). The effects of extrusion temperature and draw-down ratio are illustrated by the stress–strain curves in Figures 1 and 2, respectively. Because the draw ratio is the dominant variable, fibers with different draw-down ratio, but equal draw ratio, are compared in Figure 2. The inverse cross-sectional area of the fibers is proportional to the product of draw-down and draw ratio. Hence, the differences in ϵ_b in Figure 2 can be discussed in terms of a total draw ratio, as introduced in section 3.4. The tensile moduli of the fibers in Figure 1 are the same for the two upper curves, but differ by a factor 2 for the two lower curves (in-

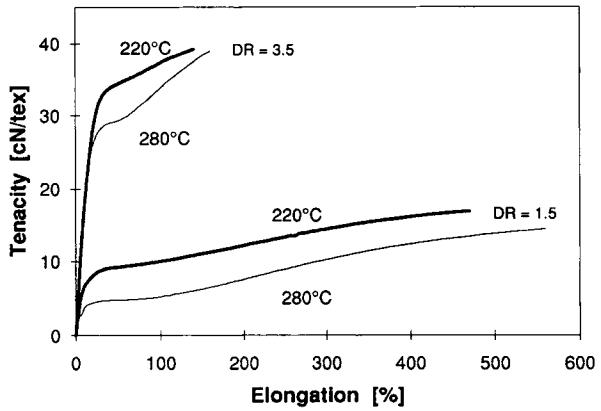

Figure 1 Stress–strain curves illustrating the effect of the extrusion temperature at high and low draw ratios. The material is a standard fiber grade with melt flow index = 14 and M_w/M_n = 5.5.

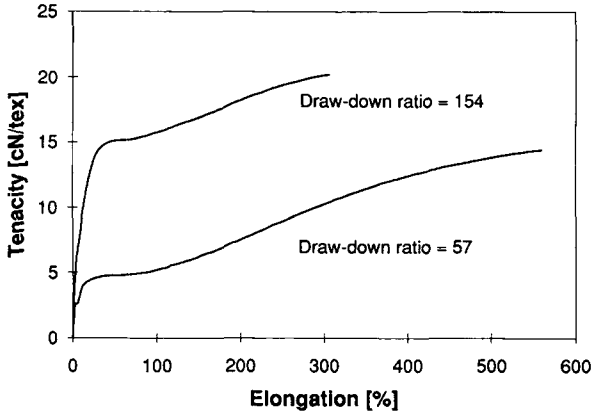

Figure 2 Stress–strain curves for fibers with different draw-down ratios, due to different extrusion rates. The draw ratio is 1.5 for both fibers, which means that the fiber diameters are different. The material is the same as in Figure 1.

creases with decreasing extrusion temperature). For the fibers in Figure 2, the tensile modulus increases with increasing draw-down ratio by a factor 2.6.

3.1.2. Drawing Stage Parameters

As expected, the draw ratio imposed in the drawing stage is the single most important processing parameter in determining the molecular orientation and, hence, the tensile properties of the fibers. The drawing temperature, on the other hand, hardly affects the mechanical properties in this study. The effect of the draw ratio is illustrated by the stress–strain curves in Figure 3, for draw ratios in the range 1.5–3.5. The tensile modulus typically increases by a factor 3–5 in this draw ratio interval, depending on the other processing parameters. At high draw ratios, all structures produced in the spinning stage are transformed into a uniaxially oriented α phase. The fraction of voids increases with increasing draw ratio. For regime I spinning parameters, the degree of crystalline perfection decreases with increasing draw ratio.

For the range of processing parameters examined in this study, the average values of ϵ_b, σ_b, and the tensile modulus of the fibers are strongly correlated. The absolute values of the correlation coefficients are all above 0.9. An (isolated) increase in any of these three entities would lead to an increase in the energy to break. However, because ϵ_b and σ_b are negatively correlated, the energy to break is not strongly correlated with the other three tensile properties. The energy to break, of course, depends on the initial diameter of the fiber. A plot of energy to break vs. draw ratio, for fibers with equal initial diameter as those in Figure 3, exhibits a minimum for draw ratios in the range 2.5–3.0, depending on the other processing parameters. This minimum might have the same explanation as the minima of the total draw ratio and the true stress at break, which are discussed in sections 3.4 and 3.5. The elastic part of the energy to break increases monotonously in the draw ratio interval examined in this study. Ziabicki[22] claimed that for drawn fibers, the elastic part of the energy to break has a maximum vs. draw ratio, while the total energy to break decreases monotonously with increasing draw ratio. Ziabicki's findings seem to be based on tensile data obtained for nylon yarns, and the fiber diameter varied according to the draw ratio (i.e., the energies were normalized by dividing by the initial cross-sectional area). Hence, these data are not fully compatible with ours.

3.1.3. Annealing Stage Parameters

The annealing stage also affects the tensile properties of the fibers. In this study we have only studied such effects in some detail for fibers with high draw ratios. As in the two former stages, the ratio of output speed to input speed has a larger effect than the temperature. The effect of the annealing ratio (defined in the Appendix) is illustrated by the stress–strain curves in Figure 4. The level of the stress–strain curve increases with increasing annealing ratio. The tensile modulus increases by 30% as the annealing ratio increases from 2 to 7%, for both draw-down ratios in Figure 4.

The effect of the annealing temperature is not

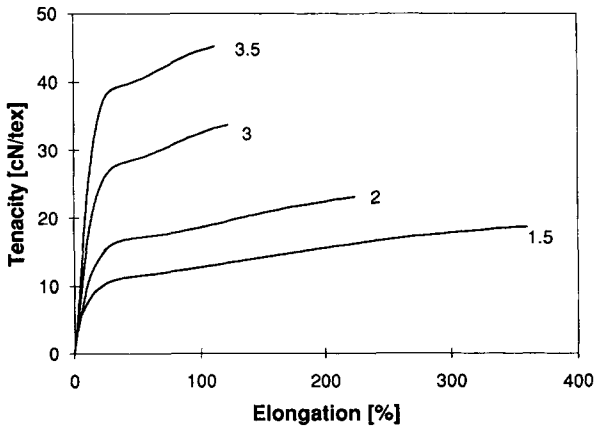

Figure 3 Stress–strain curves for 4 dtex fibers with draw ratios as indicated (because all the fibers have the same initial diameter, the draw-down ratios differ as well, but the draw ratio dominates). The fibers were drawn at 140°C. The material is the same as in Figure 1.

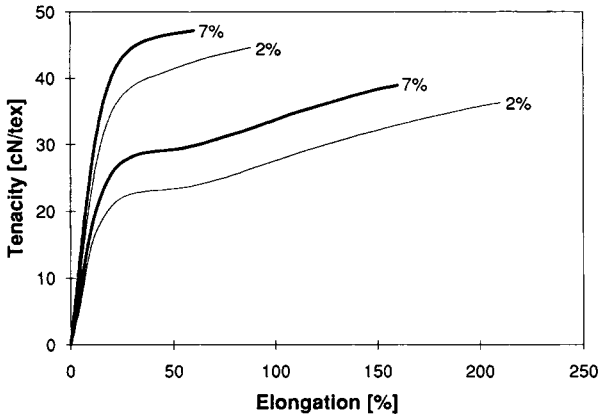

Figure 4 Stress–strain curves for fibers with different annealing ratios as indicated. The draw-down ratio is 67 for the two upper curves and 24 for the two lower curves. The draw ratio is 3.5 in all cases. The material is the same as in Figure 1.

significant at low annealing ratios. At high annealing ratios, increasing the annealing temperature has the same effect as increasing the annealing ratio. Nagou et al.[23] reported the opposite effect: the dynamic tensile modulus E′ of cold-drawn and subsequently annealed PP films decreased with an increase in the annealing temperature, while the crystallinity, the density, and the thickness of the crystalline layer increased. Nagou et al. explained this by a decrease in the volume fraction of tie molecules.

In our study, annealing-induced increases in tensile modulus and strength are accompanied by radial sharpening in the WAXS diagrams, and decreased orientation in noncrystalline regions, as measured by IR dichroism. Both these effects, the perfection of crystalline regions and the disorientation of chain segments in noncrystalline regions, are well known, although Salem et al.[24] recently reported an increase in amorphous orientation with increasing annealing temperature, for high-speed spun PET fibers. Annealing stage parameters do not affect the degree of bimodality significantly. Lentz et al. and others[25,26] observed that a population of crystallites with the chain axis oriented perpendicular to the fiber axis was formed during annealing of uniaxially oriented PP fibers and films.

3.2. Effects of the Molecular Weight Distribution

This section will deal with some effects of the weight average molecular weight (M_w) and the width of the molecular weight distribution (M_w/M_n) on the structure development, and on the tensile properties. The effect of M_w is well known. The time needed for molecular relaxation increases with increasing M_w. Hence, for a given set of processing conditions, the efficiency of the spinning and drawing stages, in producing molecular orientation, increases with increasing M_w. This explains why the level of the stress–strain curve increases with increasing M_w. Modifications that lead to an increase in σ_b, only via increased orientation, also lead to a decrease in ϵ_b. However, both σ_b and ϵ_b increase with increasing M_w in this study. The molecular orientation increases with increasing M_w, but the maximum draw ratio of chains ($\propto \sqrt{M}$)[27] also increases, and the effect of the latter on ϵ_b seems to dominate. In a similar study by Gill and Benjamin,[10] ϵ_b decreased with increasing M_w. Smith et al.[15] compared PE fibers with the same tensile modulus, i.e., molecular orientation. They found that both σ_b and ϵ_b increased with increasing M_w.

The effect of the polydispersity index, M_w/M_n, is more complicated. The narrow molecular weight distributions (MWD) in our study are so-called controlled rheology (CR) grades, which are prepared by peroxide degradation. Triacca et al.[28] have discussed the effect of peroxide degradation on the MWD of PP. The main effects are the narrowing of the distribution and the removal of the high molecular weight tail. The effect of polydispersity on the structure development in the spinning stage is different from that in the drawing stage. In our study, the spinning stage is in regime I for the broad distributions ($M_w/M_n > 5.5$), and in regime II for the narrow distributions ($M_w/M_n < 3.5$), for all examined combinations of spinning stage parameters and M_w. (Some of the processing conditions that were used for intermediate distributions could not be applied to narrow and broad distributions.) Similar trends have been reported by Fan et al.[5]

However, in studies involving higher draw-down ratios and higher spinning velocities (i.e., long-spin processes), the highest molecular orientation was achived for narrow distributions.[2,4] According to Kloos,[4] this is because grades with narrow and broad molecular weight distributions have different elongational viscosity vs. elongation rate. However, our observations might also be explained by local effects, i.e., solidification induced by strained high molecular weight chains. In the high-speed study by Kloos,[4] bimodal orientations are only observed for broad distributions, just as in our study. This must be because the high molecular weight tail and the low molecular weight tail experience different (molecular) stresses in the spinline, which allow for local morphological variations. The former experience the highest stress, crystallize first, and carry the load so

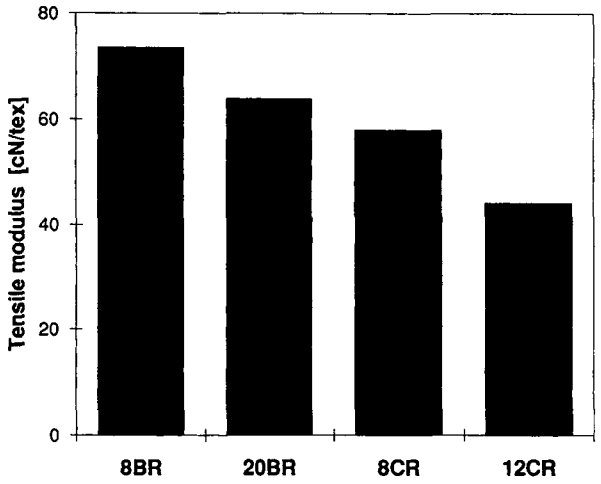

Figure 5 Tensile moduli of 11 dtex fibers with draw ratio 1.5 and draw-down ratio 57. "BR" denotes a broad MWD, "CR" denotes a narrow (controlled rheology) MWD, and the number in the coordinate code is the melt flow index.

that the latter can crystallize in a relatively relaxed state, forming the secondary population, cf. the discussion of bimodality in section 3.1.1. In conclusion, the structure development in the spinning stage depends on the apparent elongational viscosity, but also on the polydispersity *per se*. The former is a function of the entire MWD, and determines the molecular orientation of the fiber. The latter can influence the homogenity of the fiber, e.g., by the formation of bimodal structures.

The spinning stage effects of M_w and M_w/M_n on the tensile properties are most clearly seen for the tensile modulus of fibers with low draw ratios, as in Figure 5: for a given M_w/M_n, the tensile modulus increases with decreasing melt flow index (or increasing M_w). For a given M_w, the tensile modulus increases with increasing M_w/M_n. For other mechanical properties, or higher draw ratios, the situation is more complicated, due to the effect of polydispersity on the drawing mechanism.

The main differences between the deformation in the drawing stage and that in the spinning stage are the "morphology" of the medium, the temperature, and the elongation rate. A lower temperature corresponds to a higher elongation rate. Both the temperature and the elongation rate are lower in the drawing stage. However, because the deformation in the drawing stage is more effective, its rate is higher relative to the effective molecular relaxation time. If the elongational deformation of the spinning and drawing stage can be compared, the ratio of deformation efficiency for narrow distributions to that for broad distributions is expected to be higher in the latter stage, based on the discussion above. This is consistent with our observations as detailed below:

As the draw ratio increases, the tensile moduli of fibers of narrow distributions increase relative to those of broad distributions. For the highest draw ratios, the effect of polydispersity shown in Figure 5 is reversed. The elongation during testing can be considered as a continuation of the deformation in the drawing stage. Typical stress–strain curves for fibers with different polydispersity are shown in Figure 6. The fiber with the broad MWD has the highest tensile modulus (the draw ratio is low as in Fig. 5), but the lowest σ_b. For all the combinations of processing parameters and M_w values examined in this study, the fibers with narrow MWD have higher σ_b and lower ϵ_b than those with broad MWD.

The main difference in stress–strain behavior between fibers of broad and narrow molecular weight distributions occurs after the yield elongation (Fig. 6). For all processing parameters and M_w values, the stress–strain curves for fibers of narrow distributions are steeper in this region, i.e., the strain-hardening effect is more pronounced. This suggests a more homogeneous deformation,[29,30] which could explain the higher average molecular orientation obtained for a given elongation in the drawing stage, as well as during testing. Smith et al.[15] compared PE fibers with different M_w and M_w/M_n, but the same tensile modulus. They found that σ_b was higher for a fiber with lower polydispersity, even though both M_n and M_w were lower, the latter by a factor 10. They explained this by a more homogeneous

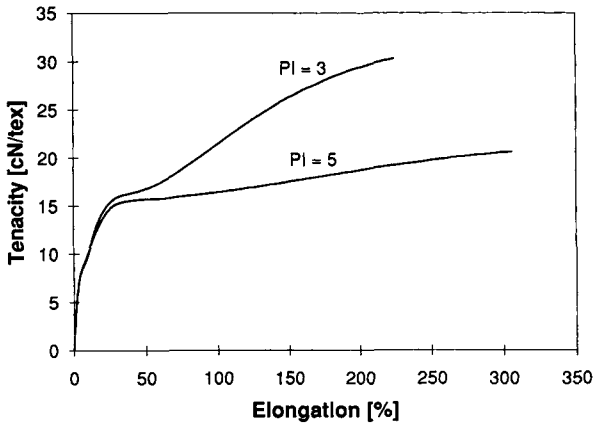

Figure 6 Stress–strain curves for fibers with different polydispersity index (PI = M_w/M_n) as indicated. The draw ratio is 1.5 for both fibers. The tensile moduli are 150 and 141 cN/tex for the broad and narrow distribution, respectively.

drawing, which resulted in a higher and more even distribution of load-bearing tie molecules. In contrast to this, Hallam et al.,[31] in a similar study, concluded that the tensile strength could be expressed as the weight-average of the tensile strengths of the molecular weight fractions present.

The deformation of the broad MWD fiber in Figure 6 tends towards necking, but it is not a true necking according to the Considère construction.[29] Inhomogenous deformation can be caused by variations in effective cross-sectional area or variations in material properties along the fiber. Fan et al.[5] reported higher diameter variations for regime I as-spun fibers of broad distributions than for regime II fibers of narrow distributions. Note that the energy to break is about the same for the two fibers in Figure 6. The difference might be that a large fraction of the chains contribute almost equally to the deformation resistance for the narrow MWD, while the high molecular weight fraction dominates for the broad MWD.

Only average values of ϵ_b and σ_b have been discussed above. The distributions of these properties[32] are also important for many applications, as well as for process control. Pompo et al.,[33] for instance, showed that ϵ_b and σ_b of poly(ethylene terephtalate) fibers are distributed according to Weibull statistics, and correlated the Weibull parameters to the process and to the fiber morphology. Marcher[34] compared the short-spin and the long-spin process for PP fibers, and found a higher coefficient of variation for the mechanical properties of fibers made by the former process, due to the turbulent cooling air and the large number of fibers emerging from the spinneret. Samuels[35] studied effects of strain rate, temperature, and orientation prior to testing on the distribution of true stress at break of PP films. According to Samuels, different flaw distributions might cause failure, depending on the strain rate and temperature.

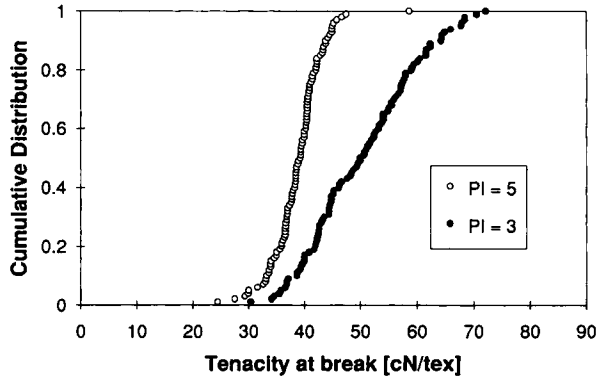

Figure 7 Cumulative distributions of tenacity at break for 100 parallels of two fibers with different polydispersity index. For both fibers the melt flow index is 8 and the draw ratio is 3.

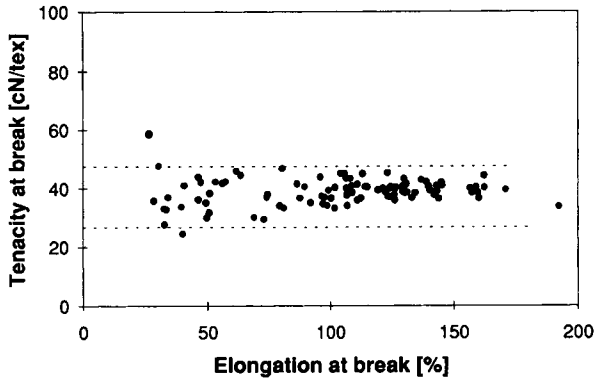

Figure 8 Tenacity at break vs. elongation at break for the parallels of the fiber in Figure 7 with broad MWD.

Among the fibers with high draw ratios in our study, narrow MWD fibers have much broader distributions of σ_b than broad MWD fibers. This is illustrated by the cumulative distributions in Figure 7. Narrow MWD fibers with high draw ratios have broader distributions of ϵ_b as well, although the difference is smaller in this case. More information about the differences in Figure 7 can be obtained by plotting tenacity at break vs. elongation at break for the parallels of the broad and narrow MWD fiber (Figs. 8 and 9, respectively). In Figure 8, the correlation is almost zero, while the correlation coefficient for the data in Figure 9 has the value −0.8. The distributions of σ_b differ less for a given ϵ_b (than in Fig. 7), especially for ϵ_b values below 100% (in Fig. 8 the distribution of σ_b seems to broaden as ϵ_b decreases). The MWD effects shown in Figures 8 and 9 are observed for all fibers with draw ratio 3

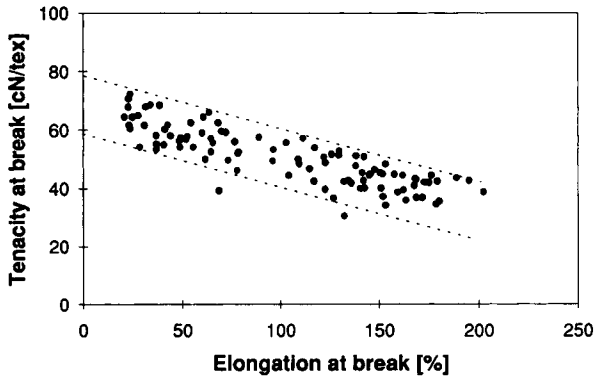

Figure 9 Tenacity at break vs. elongation at break for the parallels of the fiber in Figure 7 with narrow MWD.

and higher. The correlation between ϵ_b and σ_b for a set of parallels, and the effect of their distributions on the tensile response of fiber assemblies, will be discussed in a forthcoming article.

The distribution of σ_b also broadens somewhat with increasing draw ratio. For the samples in Figure 3, the standard deviation increases from 1.2 to 2.6, but the coefficient of variation is almost the same. Amornsakchai et al.[12] observed a broadening with increasing draw ratio for PE fibers.

3.3. Empirical Expressions for the Tensile Properties

The data from our study were analyzed statistically. One result from these analyses was a set of models for this fiber line, relating mechanical properties to processing parameters and MWD. Good predictions of the tenacity at break were obtained with a linear function of the deformation ratios and temperatures along the fiber line, the melt flow index, and the polydispersity index. The most important parameter is, of course, the draw ratio. The predictions of tenacity at break for fibers with high draw ratios and narrow MWD are somewhat too low. A similar model for the tensile modulus is also acceptable, but the explained variance is lower. There are several reasons for this: there is more noise in the data, the tenacity at break is more dominated by the draw ratio, and the correlation between tensile modulus and polydispersity varies with the draw ratio, as discussed in section 3.2. The latter effect can be included in a more complicated model with crossterms.

A simple linear model is not acceptable for the elongation at break. In a plot of predictions vs. measurements, the points do no follow a linear trend. The predictions are clearly too low for low and high values of the elongation at break, and too high in the intermediate region. However, a linear model for the total draw ratio,

$$\lambda_t = \lambda_d \lambda_b, \qquad (1)$$

where λ_d is the draw ratio of the drawing stage and $\lambda_b = 1 + \epsilon_b$, does not have this problem. The spinning stage deformation is neglected in Eq. (1). A model for the elongation at break, found by rearranging the model for λ_t, is just as good as the one for the tensile modulus.

None of the models above are acceptable for the energy to break. A model with acceptable prediction, considering the noise in these data, has been found by careful selection of crossterms (the total number of terms is about the same as in the models described above). However, the physical basis of this model is unclear. There is a risk of over-fitting for such data sets, but the cross-validation procedure implemented in the statistical software should prevent this.

3.4. Total Draw Ratio

Smith et al.[27] published values for the maximum draw ratio of polymer molecules initially in the unperturbed (θ) state. According to Smith et al., these maximum (molecular) draw ratios apply to all specimens of flexible polymers, regardless of their state of aggregation. However, in practice, the efficiency of the (macroscopic) deformation is never 100%. On the other hand, all the chains will not have reached their maximum draw ratio at fracture; the average distance along a chain between two "clamping points" is less than the chain length. At a high elongation rate the deformation is more effective, but the average molecular draw ratio at break will be lower. According to Samuels,[35] the elongation at break is nearly independent of initial orientation at very high elongation rates (much higher than in our study). At these rates there will be no time for molecular reorganization. Hence, the elongation at break is low and directly determined by the weakest link of the original morphology. At low and intermediate rates, the elongation at break decreases with increasing initial orientation, as in our study. Sa-

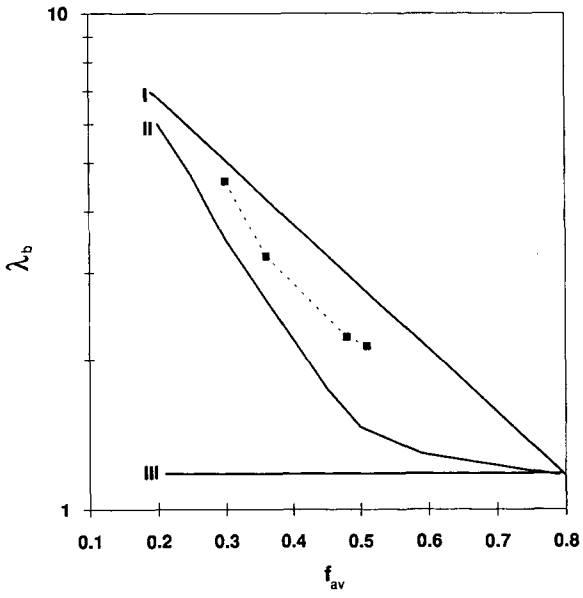

Figure 10 Strain fracture envelope ($\lambda_b = 1 + \varepsilon_b$ and f_{av} is the average Hermans–Stein orientation factor of crystalline and noncrystalline phases). Solid lines are schematical representations of Samuels' data[35] for different deformation rates: 1–50 %/min (I), 10^3 %/min (II), and 10^6 %/min (III). Data for series B in Figure 11 (500 %/min) are shown as squares.

muels' observations are shown schematically in Figure 10.

As mentioned above, the maximum molecular draw ratio is related to the molecular weight ($\propto \sqrt{M}$). Hence, for fibers of a given polymer grade, but with different processing histories, variations in the total draw ratio must be due to (1) different degrees of degradation, (2) different elongation rates relative to molecular relaxation times during processing as well as during testing, and/or (3) different distributions of flaws leading to fracture. The first of these causes can be neglected, cf. section 2. For a given polymer grade, our data indicate that the second cause dominates.

The efficiency of the draw-down ratio is low, due to the rapid molecular relaxation at this high temperature. The effective deformation ratio of the spinning stage is difficult to quantify. If the draw-down ratio is neglected, the total draw ratio can be written as in Eq. (1). Figure 11 shows λ_t, calculated by Eq. (1), vs. draw ratio, for fibers with different extrusion temperature and diameter prior to testing (Series A and B). The applied draw-down ratio decreases with increasing draw ratio for a given diameter prior to testing. The total draw ratios of 11 dtex fibers are higher than those of 4 dtex fibers in Figure 11. One possible reason for this is that 11 dtex fibers have a lower draw-down ratio (and molecular orientation), and, hence, less spinning stage deformation is neglected by using Eq. (1). Fibers with different diameters prior to testing also have different fractions of the total draw ratio left for the testing. Hence, different efficiencies during drawing and testing can be responsible for the effects of initial diameter in Figure 11. The efficiency of one stage might also depend on the morphology and orientation formed in the preceding stage. There might be an effect of the diameter *per se* as well. This could be examined by testing fibers with different diameters, but equal degree of orientation. Studies of this kind have been reported for PE fibers, focusing on the tensile strength. Some researchers report that the tensile strength depends on the diameter,[12] while others claim that it is independent of the diameter.[36]

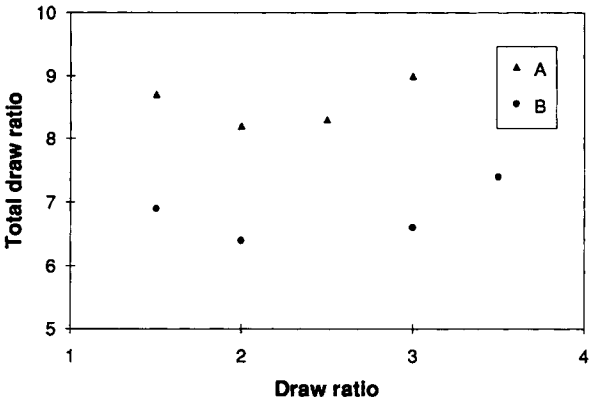

Figure 11 Total draw ratio, as given by Eq. (1), vs. draw ratio. The two series differ in extrusion temperature and linear density prior to testing. Series A: 11 dtex fibers with extrusion emperature 220°C, series B: 4 dtex fibers with extrusion temperature 280°C. For a given linear density, the draw-down ratio decreases with increasing draw ratio. The fibers with linear density 4 dtex are the same as in Figure 3. The polymer grade is the same as in Figures 1–4.

The ratio of λ_t of fiber B to that of fiber A in Figure 11 is almost independent of draw ratio ($\lambda_t^B/\lambda_t^A \approx 0.8$). Because the inverse cross-sectional area is proportional to the product of the draw-down ratio and the draw ratio, the ratio of the draw-down ratios of the two series is the same for all draw ratios ($\lambda_s^A/\lambda_s^B = 4/11 \approx 0.4$). Assume that all fibers have the same true (molecular) total draw ratio,

$$\lambda_{tt} = \beta\lambda_s\lambda_t, \tag{2}$$

where β is the overall deformation efficiency. This implies that

$$\lambda_t^B/\lambda_t^A = \beta^A\lambda_s^A/\beta^B\lambda_s^B, \tag{3}$$

i.e., $\beta^A/\beta^B \approx 2$. This ratio of efficiencies was expected to be larger than unity because 11 dtex (A) fibers experience a larger fraction of the total draw ratio outside the spinning stage than 4 dtex fibers; hence, the overall efficiency for 11 dtex fibers is higher. Also, the extrusion temperature was 280°C for B fibers and 220°C for A fibers. This is consistent with a higher deformation efficiency for the latter fibers. Data for which only one processing parameter is varied confirm this: for fibers with draw ratio 1.5 and 3.5, regardless of diameter prior to testing, we find that $\beta^{220°C}/\beta^{280°C} \approx 1.2$ and 1.1, respectively. When only the diameter prior to testing is varied we find that $\beta^{11dtex}/\beta^{4dtex} \approx 1.5$.

The last detail to discuss is the minima in Figure 11. Because the draw-down ratio is neglected in Eq. (1), λ_t was expected to increase with increasing draw ratio (i.e., decreasing draw-down ratio for a given linear density prior to testing). However, λ_t has a distinct minimum vs. draw ratio. This might be explained by the strain fracture envelope shown in Figure 10. At low orientation levels, λ_b decreases more rapidly for intermediate deformation rates than for low rates. This could be because the effective elongation rate increases with increasing draw ratio, due to lower molecular mobility. At high orientation levels the situation is reversed, as the curve

for the intermediate deformation rate approaches the horizontal high elongation rate asymptote. The decrease of λ_t vs. draw ratio in Figure 11 can also be caused by different deformation efficiencies during drawing and testing.

3.5. Diameter and True Stress at Break

The deformation is usually assumed to be incompressible. Hence, the cross-sectional area at break is related to the inital area and the elongation at break in the following way:

$$A_b = A_o/(1 + \epsilon_b). \quad (4)$$

Hamza et al.[37] studied the cross-sectional area of PP fibers vs. draw ratio by interferometry, and suggested an empirical expression that was a slight modification of Eq. (4). If Eq. (4) is applied to the fibers in Figure 11, A_b increases from 1 to 2 dtex with increasing draw ratio for the fiber with initial linear density 4 dtex, and from 2 to 4 dtex for the 11 dtex fiber. The increase with increasing draw ratio is, of course, due to the increasing initial degree of molecular orientation, via decreasing ϵ_b. Fibers with different dimension prior to testing will only have the same A_b if the difference in initial dimension exactly match the difference in remaining total draw ratio, i.e., if both fibers have been deformed with the same efficiency during processing. As stated in section 3.4, this is not so in our case, due to different extrusion temperatures. This explains why A_b of the 11 dtex fibers are higher than that of the 4 dtex fibers; the denominator in Eq. (4) is too small relative to that of the 4 dtex fiber.

Samuels[35] showed that PP films and fibers that were deformed at a low rate fractured at the same true stress, irrespective of the initial degree of orientation. Due to the molecular reorganization, the specimens were in the same structural state at fracture. Similarily, Takaku[38] studied the creep fracture of PP fibers with different draw ratios and diameters. In a plot of tenacity at break vs. time to break, there was one curve for each draw ratio. However, in a similar plot of true stress, data for all draw ratios condensed on a single curve. In his study, Samuels[35] considered a range of elongation rates, below and above the one used in our study (Fig. 12). At very high elongation rates, the true stress increased with increasing initial molecular orientation, i.e., the orientation at break was close to the initial orientation. At intermediate elongation rates, the true stress at break had a minimum vs. initial orientation. The reason for the decrease in true stress at break at

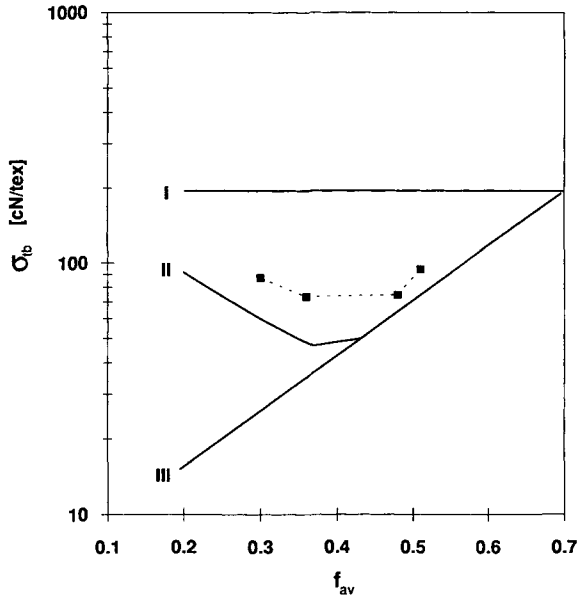

Figure 12 True stress fracture envelope (f_{av} is the average Hermans–Stein orientation factor of crystalline and noncrystalline phases). Solid lines are scaled schematical representations of Samuels' data[35] for different deformation rates: 1–50 %/min (I), 10^3 %/min (II), and 10^6 %/min (III). Data for series B in Figure 11 (500 %/min) are shown as squares.

these rates is probably the change in effective elongation rate, as described in section 3.4.

If Eq. (4) is valid, the true stress at break is

$$\sigma_{tb} = \sigma_b(1 + \epsilon_b). \quad (5)$$

This is the relation that was used by Samuels and Takaku. If σ_{tb} is plotted vs. draw ratio for the fibers in Figure 11, the result will, in fact, be very much like Figure 11. From a comparison of Eq. (1) and Eq. (5), the resemblance with Figure 11 could be expected, because λ_d and σ_b are highly correlated, and for a given λ_d, the two series in Figure 11 have almost the same σ_b (but 4 dtex fibers have significantly higher tensile modulus and molecular orientation).

Our results for the true stress vs. draw ratio are consistent with Samuels' observations at similar elongation rates,[35] cf. Figure 12. The minima vs. draw ratio, as well as the difference between series A and B fibers, can be explained by different effective deformation rates. However, there are alternative explanations. There might, for instance, be a skin–core variation in load-bearing chains near break. Some other possibilities are mentioned in section 3.4.

4. SUMMARY AND CONCLUSION

The results reported in this study are based on a total of about 80 PP fibers. The span in MWD and processing parameters was made as large as possible—the limiting factor being the processability of the polymer—and it should cover most of the relevant industrial processing conditions. However, fibers with smaller or larger diameters are used for some applications. For instance, in nonwoven fabrics for hygienic applications, fibers with linear density close to 2 dtex and low draw ratios are used. We are currently studying the properties of such fibers.

The most interesting observation made in this study is perhaps the differences observed regarding the distributions of tenacity and elongation at break. These distributions—not only the mean values—influence the mechanical properties of products made of these fibers, such as nonwoven fabrics. What we have seen is that for high draw ratios, a narrow MWD leads to a broader distributions of ultimate tensile properties than a broad MWD. In addition, fibers with narrow MWD and high draw ratios have a clear negative correlation between tenacity and the elongation at break. For fibers with high draw ratios and broad MWD, these two quantities are much less correlated.

Of course, mean values of tenacity and elongation at break, in addition to the average tensile modulus, are important quantities in characterizing the mechanical properties of the fiber. An increase in average molecular weight lead to an increase in all of these properties. Changes in the width of the MWD, however, caused different changes in the mechanical properties, depending on the value of the draw ratio in the drawing stage of the process. At low draw ratios, broad MWD fibers had the highest tensile modulus and elongation at break, and the lowest tenacity at break. Increasing the draw ratio lead to an increase in the tensile modulus and the tenacity at break, and a decrease in elongation at break, for both broad and narrow MWD fibers. However, the increase in tensile modulus was larger for the narrow MWD fibers, so that for high draw ratios such a fiber had, in fact, a higher tensile modulus than a broad MWD fiber.

The mechanical properties measured in this study agreed well with what one would expect from the morphological characteristics obtained by WAXS and IR dichroism analyses. The main effect is that higher stress in the spinning or drawing stage, cased by either an increase in deformation rate or a decrease in temperature, leads to a higher degree of molecular orientation and, hence, increased tensile stiffness and strength. However, the details reveal a more nuanced picture. After the spinning stage, all broad MWD fibers had what we called a type I structure, and all narrow MWD fibers had a type II structure. The type I structure is a monoclinic α phase with bimodal orientation, and the type II structure is a uniaxially oriented mesomorphic phase. This difference in structure is mainly due to the difference in the high molecular weight tail of the MWD. However, the degree of orientation of the polymer segments in both the crystalline and noncrystalline regions is a function of the spinline stress, which is determined by the elongational viscosity of the polymer melt. The rate dependence of this viscosity and, hence, the effect of draw-dawn ratio (and draw ratio) on the molecular orientation, is a function of the entire MWD. At high draw ratios, all structural entities produced in the spinning stage were transformed into a uniaxially oriented α phase.

Several important questions clearly require further studies. More detailed information about the structure development during processing and testing is needed in order to understand the deformation efficiency in the various stages of the process, and how this relates to the diameter and true stress at break. A more detailed description of the fracture mechanisms is also needed. The morphology at break (orientation of chains, types of defects, density, and shape of voids, etc.) is a key element in order to clarify some of the issues brought up in this article. Skin–core effects, e.g., cross-sectional variations of molecular orientation, residual stress or degradation, might also influence the mechanical properties of fibers.

This paper is based on results from the "Expomat Fiber Project," supported by Statoil and The Research Council of Norway. The authors wish to thank Terje Svendsen at Statoil for doing the tensile testing.

APPENDIX: LIST OF DEFINITIONS AND SYMBOLS

Definitions

Short-Spin vs. Long-Spin Processes

In the former process, a larger number of filaments is extruded through the spinneret. The velocity of the cooling air is higher (usually turbulent), while spinning velocities and draw-down ratios are lower. Hence, the spinning length is shorter. These two processes are also known as compact and conventional spinning, respectively.

Spinning Stage Parameters

The polymer melt exits the spinneret at a certain *extrusion velocity* and *extrusion temperature*. At a given distance below the spinneret the filaments are pulled at a certain velocity—the *spinning velocity*. The ratio of spinning velocity to extrusion velocity is called the *draw-down ratio*.

Drawing Stage Parameters

The *draw ratio* is equal to the ratio of output velocity to input velocity for the drawing stage. For the integrated short-spin line considered in this article, the input velocity of the drawing stage is equal to the spinning velocity. The *drawing temperature* can also be adjusted.

Annealing Stage Parameters

The *annealing ratio* is defined as the difference between input velocity and output velocity speed for the annealing stage, divided by input velocity. Annealing is performed at a certain *temperature*. The output velocity of the annealing stage is often called the *line velocity*, and is the speed at which the final fiber emerges from the fiber line.

Tex

A measure of linear density; 1 tex = 1 g/km. The cross-sectional area of the fiber is equal to the ratio of bulk density to linear density, and is proportional to the ratio of extrusion velocity to line velocity.

Tenacity

Nominal stress of fibers is usually called tenacity when it is measured as load divided by linear density, e.g., with units N/tex.

Symbols

A_b Cross-sectional area of fiber at break.
A_o Cross-sectional area of a fiber prior to testing.
M_n Number-average molecular weight.
M_w Weight-average molecular weight.
α Denotes the monoclinic crystal structure of polypropylene.
β Overall deformation efficiency of the spinning and drawing stages, as defined by Eq. (2).
ε_b Elongation at break.
λ_b $1 + \varepsilon_b$.
λ_d Draw ratio.
λ_s Draw-down ratio.
λ_t The "total" draw ratio of a fiber when the spinning stage is neglected. Defined as the product of λ_b and λ_d.
λ_{tt} True molecular draw ratio. Defined as the product of β, λ_s, and λ_t.
σ_b Tenacity (nominal stress) at break.
σ_{tb} True stress at break

REFERENCES

1. I. Diacik, Jr., I. Diacik, and M. Jambrich, *Acta Polym.*, **41**, 500 (1990).
2. F.-M. Lu and J. E. Spruiell, *J. Appl. Polym. Sci.*, **34**, 1521 (1987).
3. F.-M. Lu and J. E. Spruiell, *J. Appl. Polym. Sci.*, **34**, 1541 (1987).
4. F. Kloos, in *Proceedings of the 4th Int. Conf. Polypropylene Fibres and Textiles*, Nottingham, UK, 1987.
5. Q. Fan, D. Xu, D. Zhao, and R. Qian, *J. Polym. Eng.*, **5**, 95 (1985).
6. H. Bodaghi, J. E. Spruiell, and J. L. White, *Int. Polym. Process.*, **3**, 100 (1988).
7. K. Hahn, J. Kerth, R. Zolk, D. Schwahn, T. Springer, and J. Kugler, *Macromolecules*, **21**, 1541 (1988).
8. I. Diacik, O. Durcova, I. Diacik, Jr., and M. Mitterpachova, *Acta Polymerica*, **39**, 391 (1988).
9. M. Nurul Huda, S. Bauer, H. Dragaun, and P. Skalicky, *Colloid Polym. Sci.*, **262**, 110 (1984).
10. R. A. Gill and C. Benjamin, *Plastics Rubbers Process.*, **5**, 25 (1980).
11. H. P. Nadella, J. E. Spruiell, and J. L. White, *J. Appl. Polym. Sci.*, **22**, 3121 (1978).
12. T. Amornsakchai, D. L. M. Cansfield, S. A. Jawad, G. Pollard, and I. M. Ward, *J. Mater. Sci.*, **28**, 1689 (1993).
13. I. M. Ward, *Plast. Rubber Compos. Process. Appl.*, **19**, 7 (1993).
14. M. A. Hallam, D. L. M. Cansfield, I. M. Ward, and G. Pollard, *J. Mater. Sci.*, **21**, 4199 (1986).
15. P. Smith, R. J. Lemstra, and J. P. L. Pijpers, *J. Polym. Sci. Polym. Phys. Ed.*, **20**, 2229 (1982).
16. F.-M. Lu and J. E. Spruiell, *J. Appl. Polym. Sci.*, **49**, 623 (1993).
17. L. Rebenfeld, in *Encyclopedia of Polymer Science and Engineering*, 2nd Ed., Vol. 6, Wiley, New York, 1989, p. 659.
18. A. Peterlin, in *Flow-Induced Crystallization in Polymer Systems*, R. L. Miller, Ed., Gordon and Breach, New York, 1977.
19. K. Katayama, T. Amano, and K. Nakamura, *Kolloid-Z. Z. Polym.*, **226**, 125 (1968).

20. B. Lotz and J. C. Wittmann, *J. Polym. Sci. Polym. Phys. Ed.*, **24,** 1541 (1986).
21. S. Brückner, S. V. Meille, V. Petraccone, and B. Pirozzi, *Prog. Polym. Sci.*, **16,** 361 (1991).
22. A. Ziabicki, *Fundamentals of Fibre Formation,* Wiley, London, 1976.
23. S. Nagou and S. Oba, *J. Macromol. Sci.-Phys.*, **B18,** 297 (1980).
24. D. R. Salem and H.-D. Weigmann, *J. Polym. Sci. Polym. Phys. Ed.*, **29,** 765 (1991).
25. J. Lenz, J. Schurz, and E. Wrentschur, *Acta Polymerica,* **35,** 74 (1984).
26. I. Masada, T. Okihara, S. Murakami, M. Ohara, A. Kawaguchi, and K.-I. Katayama, *J. Polym. Sci. Polym. Phys. Ed.*, **31,** 843 (1993).
27. P. Smith, R. R. Matheson, Jr., and P. A. Irvine, *Polym. Commun.*, **25,** 294 (1984).
28. V. J. Triacca, P. E. Gloor, S. Zhu, A. N. Hrymak, and A. E. Hamielec, *Polym. Eng. Sci.*, **33,** 445 (1993).
29. I. M. Ward, *Mechanical Properties of Solid Polymers*, 2nd Ed., Wiley, New York, 1983.
30. Y. Termonia and P. Smith, *Macromolecules,* **20,** 835 (1987).
31. M. A. Hallam, G. Pollard, and I. M. Ward, *J. Mater. Sci. Lett.*, **6,** 975 (1987).
32. H. H. Kausch, *Polymer Fracture*, Springer, Berlin, 1978.
33. A. Pompo, A. D'Amore, S. Saiello, L. Nicolais, D. Acierno, R. Bianchi, and R. Vosa, *J. Mater. Sci. Lett.*, **11,** 504 (1992).
34. B. Marcher, in *Proceedings from the INDEX 93 Congress* (Session 2c), Geneva, 1993.
35. R. J. Samuels, *Structured Polymer Properties*, Wiley, New York, 1974.
36. C. W. M. Bastiaansen, *Polymer,* **33,** 1649 (1992).
37. A. A. Hamza, I. M. Fouda, K. A. El-Farhaty, and S. A. Helay, *Polym. Test.*, **7,** 329 (1987).
38. A. Takaku, *J. Appl. Polym. Sci.*, **26,** 3565 (1981).

Received October 14, 1993
Accepted December 10, 1993